Energizing Battery Research with Atomic Force Microscopy

OXFORD INSTRUMENTS
ASYLUM RESEARCH

Introduction

In order for electric vehicles, renewable energy, the internet of things, and expanding rural electrification to come online in the next decades, complementary energy storage (i.e., batteries) will be required to time-shift renewable energy generation so power is available when the sun isn't shining and the wind isn't blowing. Global demand for battery capacity is projected to increase by an order of magnitude from present levels to over 2 TWh in 2030.[1] Much of this capacity will be deployed in the massive production of electric vehicle fleets, their related charging infrastructure, mobile devices, the internet of things, and large-scale long-duration storage that will all also play a role in securing the grid, time shifting renewable solar and wind generation, and bolstering critical infrastructure against disaster and climate-change related outages.

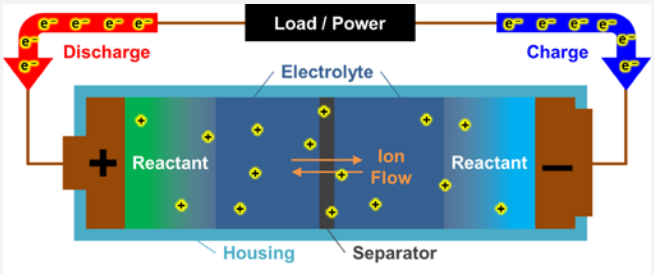

Figure 1. Schematic showing the various basic components of a battery.

What is a battery?

The word "battery" probably conjures an image of the cylindrical batteries that power everything from toys to flashlights. The more correct term for these is actually "cells" because a "battery" conventionally refers to a group of cells. Nevertheless, because cells can be stacked in series and parallel to make a battery of virtually any shape and size, one can conceptualize a battery as an equivalent larger-capacity, larger-power cell and so the terms have become interchangeable in common conversation. We will use "battery" throughout this whitepaper.

As shown in **Figure 1**, every battery has a **negative** and **positive** electrode terminal (also known as the anode and cathode, or vice versa, depending on if the battery is discharging or charging), **reactant** materials that store the electrical energy in chemical bonds inside the device, an **electrolyte** that is usually an ionically conductive fluid, a **separator** that allows ion-selective flow between anode and cathode, and a **housing** to encapsulate the entire structure against the atmosphere.

During discharge and charge, shown respectively with red and blue arrows, electrochemically-generated electrons from the reactants travel between the positive and negative electrode terminals through an external circuit (either driving a load or being driven by a power source) while complementary positive ions move through the electrolyte and separator inside the device. Research and engineering in batteries can optimize any one of those components, and is generally driven by these goals:

- increasing kWh/kg (specific energy density) or kWh/m^2 (footprint energy density)
- increasing kW/kg (specific power density) or kW/m^2 (footprint power density)
- decreasing $/kWh (specific installed cost) or $/kWh/cycle (specific installed cost per cycle)

Measuring Battery Performance

Many researchers analyze different battery chemistries and components as well as test the performance of the resulting devices using conventional electrochemical cycling techniques and spectroscopic methods. However, unique insights into battery materials and operation can come from analysis at the nanoscale, such as what is achievable with Atomic Force Microscopy (AFM). Because an AFM probe physically interacts with the surface that it is mapping, details about topographical changes, conductivity, molecular ordering, nanomechanical properties, and more, can be discerned. Historically, even with an AFM, this type of analysis has been supremely challenging with batteries because many of the critical materials involved, such as lithium, are air- and moisture-sensitive. Moreover, conventional battery architectures cannot be "examined" without disassembling them (destroying the battery and its function in the process), so innovative imaging techniques are required.

Despite the apparent difficulty, nanoscale analysis of batteries remains critical, and the AFM fills this requirement, enabling the advanced measurements described above at different levels of complexity and difficulty:

- **Ex-situ battery measurements** (straightforward, easy): taking images of relevant battery components outside of an assembled battery architecture, possibly in uncontrolled/ambient atmosphere
- **In-situ battery measurements** (complex, moderate): taking images of battery components in a chemical environment relevant for battery operation
- **Operando battery measurements** (intricate, difficult): taking images of battery components during operation, meaning charging or discharging in physically relevant chemical conditions

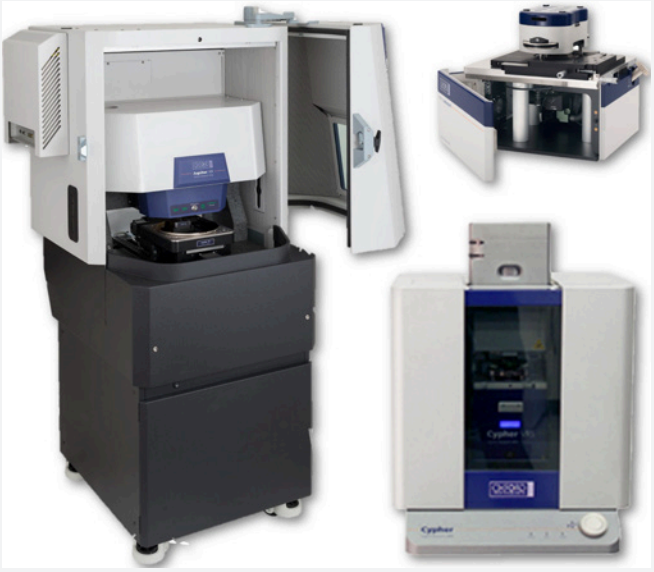

Figure 2. AFMs offered by Oxford Instruments Asylum Research for battery research

Asylum AFMs for Battery Research

Oxford Instruments Asylum Research offers three different AFM platforms for battery research (**Figure 2**). The MFP-3D is a highly versatile AFM that offers high resolution and a broad range of available accessories, including an electrochemistry cell. The Jupiter XR is a large-sample AFM that enables acquisition of images up to 100 x 100 microns on samples up to 200 mm (8 inches) in diameter while delivering ultra-high resolution and high throughput, with a suite of accessories for environmental control available

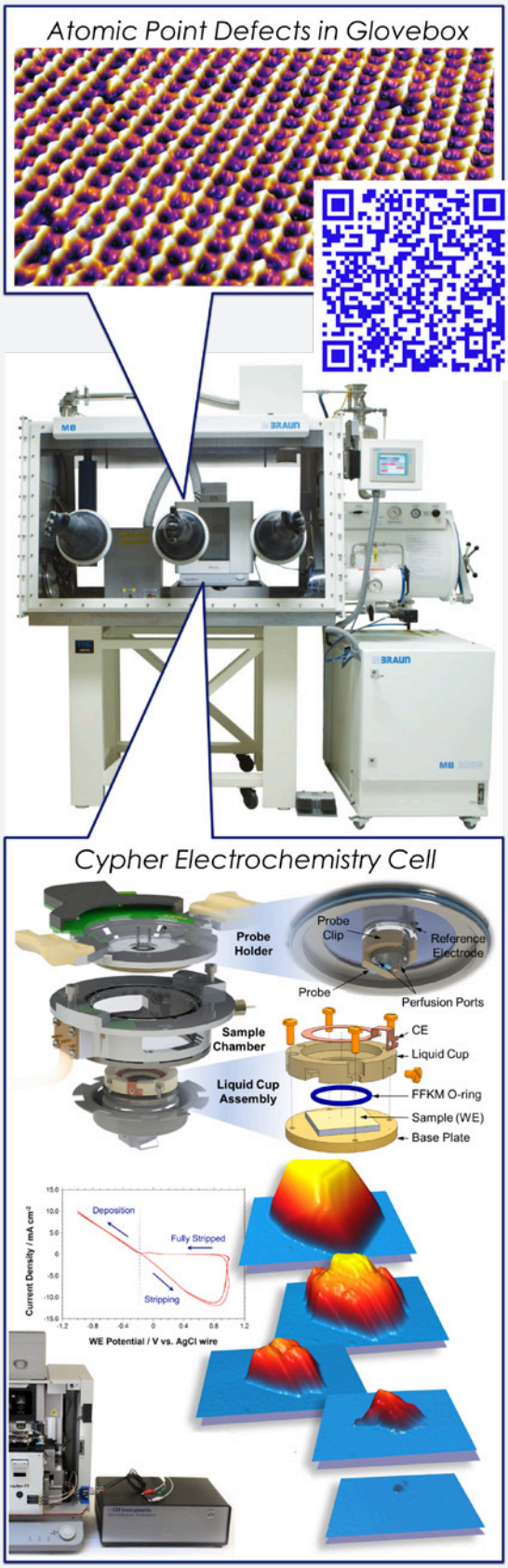

Figure 3. (Top) The Asylum Research Cypher ES AFM shown in a glovebox. (Bottom) The Cypher electrochemistry cell can be used either in a glovebox, as shown, or under ambient conditions.

and in active development. Finally, the Cypher ES provides the highest resolution and the highest speed along with the most complete environmental control for sensitive chemistries with a fully sealed sample cell and electrochemistry cell.

Many energy storage materials are air and moisture sensitive, requiring stringent control over reactor conditions that ex-situ imaging cannot provide. To reasonably conduct measurements in conditions that resemble the inside of an operating battery, one can place the AFM inside a glovebox to benefit from its controlled environment, as shown. For most AFMs, the added noise and vibration of a glovebox comes with unavoidable tradeoffs in terms of both performance and ease of use. However, the Cypher ES, which is compact for glovebox use, maintains its ease of use and ultra-high resolution performance, even with the pumps running. Scan the QR code in **Figure 3** to learn more about imaging under these conditions. Additionally, for in situ and operando measurements, where images are acquired at interfaces inside of a device, electrical contacts and voltage control must reach the reactive surfaces, and this can be accomplished by assembling an electrochemical cell inside the AFM. The Cypher ES AFM has a flexible and modular closed cell design for completeenvironmental control and liquid containment, and it supports almost any potentiostat.

Ex-situ AFM measurements

The simplest way to get started characterizing battery components with AFM is to take measurements outside of an assembled battery architecture. Certain materials (e.g. Lithium metal) are precluded from this approach due to air and moisture sensitivity, but other materials such as battery housing materials or electrode films or current collector components may be accessible if they do not require strict engineering controls. An advantage of ex-situ imaging is that virtually all AFM characterization modes are straightforward to implement in ambient conditions, opening the realm of cross-mode correlative imaging.

Example: Battery cathode materials

As a relevant ex-situ measurement example, one of the most common cathode materials for higher energy density Li-ion batteries is $LiNi_xMn_yCo_zO_2$, also known as "NMC." To explore the utility of AFM in characterizing this material, sample NMC sheet films on an Al current collector were purchased (MSE Supplies) and then characterized with the Jupiter XR AFM as-received with minimal preparation. Specifically, conductive AFM (CAFM) was used to visualize nanoscale distributions of conductivity across the sample at different length scales (100 µm, 10 µm, 1 µm), allowing current to be correlated with topographic features such as larger "boulders," interstitial grooves, and grains (**Figure 4**). It was observed that certain grains in the larger

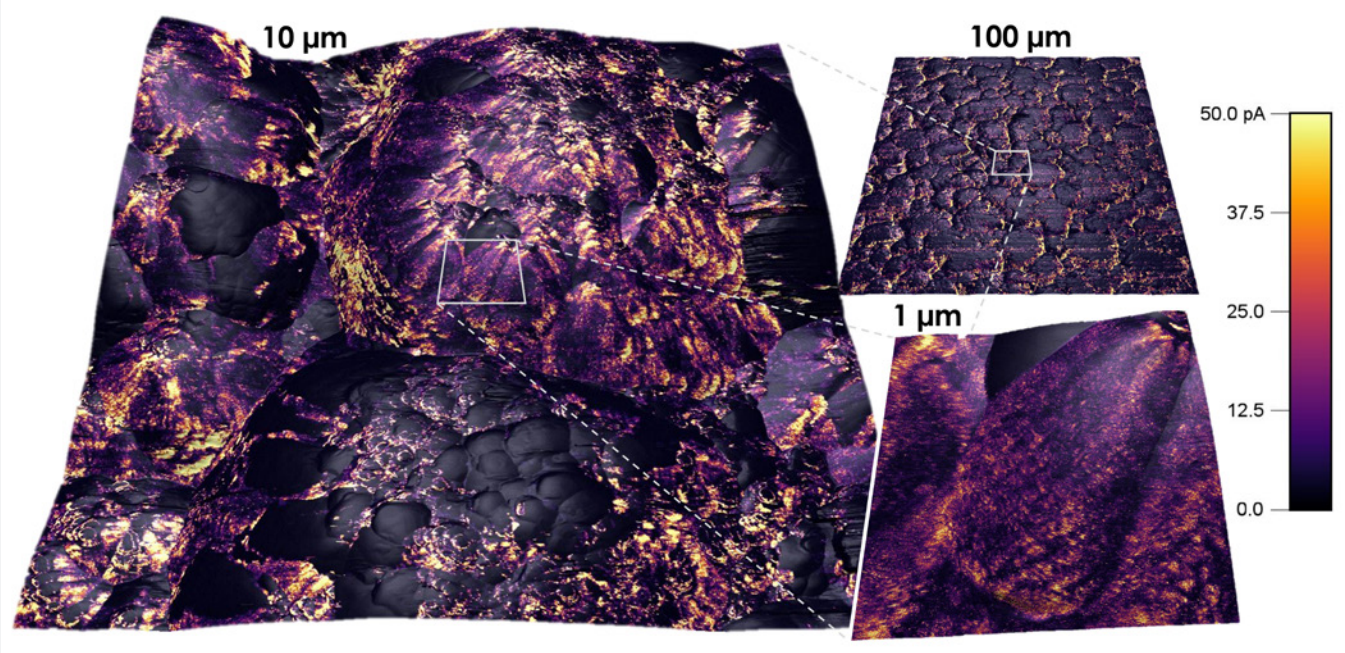

Figure 4. Current measured with conductive AFM overlaid on a 3D rendering of topography of a commercially available Li-ion battery NMC cathode.

boulders lacked conductivity, and grooves had higher conductivity than the boulders. In addition to CAFM, further electrical characterization could be pursued using Kelvin Probe Force Microscopy (KPFM) to discern the work function (volta potential) changes of the different sample features or Scanning Capacitance Microscopy (SCM) to map capacitance and ion-based doping heterogeneity in the sample. For still further characterization, nanomechanical imaging modes including AM-FM Viscoelastic Mapping Mode or Fast Force Mapping (FFM) could be used to visualize nanoscale variations in moduli, dissipation, adhesion, and indentation.

Example: Nanomechanical analysis on polymer-gel electrolyte

In another example of ex-situ AFM measurements, researchers evaluated different formulations of a hybrid polymer-gel electrolyte material with respect to both lithium salt concentration and acetonitrile as a solvent additive.[2] In **Figure 5**, two sets of data are presented that correspond to two different electrolyte compositions. For each data set, topographic map of the surface structure is provided with a corresponding force map where mechanical information has been obtained at every pixel using the AFM probe. Topographic images assess the effect of the different formulations on the morphology of the gel electrolyte, while the force maps determine its thickness and mechanical stability by measuring the forces required to rupture the film. For these measurements, plastic deformation indicates deleterious compositional effects that could result in crack formation as the volume or strain changes during lithiation/delithiation. Ultimately, the AFM measurements helped conclude that high concentrations of lithium salt and addition of acetonitrile not only increase the Li-ion storage capacity but also together stabilize the electrolyte gel by making it both thicker and more flexible.

In-situ AFM measurements

As an example of a more complex in-situ measurement, consider imaging a liquid-electrode interface—that is, the surface(s) where the electrochemical reaction(s) critical to the battery will take place—under voltage and environmental control. This concept translates beyond energy storage to catalysis, biosensors, and other electrochemical technologies, but it is an especially important concept for batteries that develop a solid electrolyte interphase (SEI) during cycling. The SEI is a passivating layer that forms on the electrode surfaces during battery charge and discharge and influences the interfacial performance of the anode and cathode, impacting a battery's capacity, discharge kinetics, and long-term stability. A key overarching feature of in-situ experiments is that during the electrochemical processes of interest, not only do electrons and ions migrate around, but the electrode surface of interest may also change conformation—different nanostructures, phase separations, crystalline lattices, and more might arise.

Example: Visualizing SEI formation

For Li-ion batteries, the electrodes are often carbon-based materials or composites. A recent in-situ AFM study used the Cypher ES and a modified electrochemical cell to explore the nucleation and growth of the SEI from 1M $LiPF_6$ in 50/50 EC/DMC as the electrolyte solution on three different electrodes: highly oriented pyrolytic graphite (HOPG), MesoCarbon MicroBeads graphite (MCMB), and non-graphitizable amorphous carbon (Hard Carbon).[3] In addition to the observation that SEI formation occurred at different potentials for each electrode material, the SEI was uniformly deposited on the circular features of the MCMB and Hard Carbon surfaces (**Figure 6**, see the topography and added roughness in Amplitude shift), while being preferentially formed at step edges for HOPG. The SEI was stable after the first cycle in all cases.

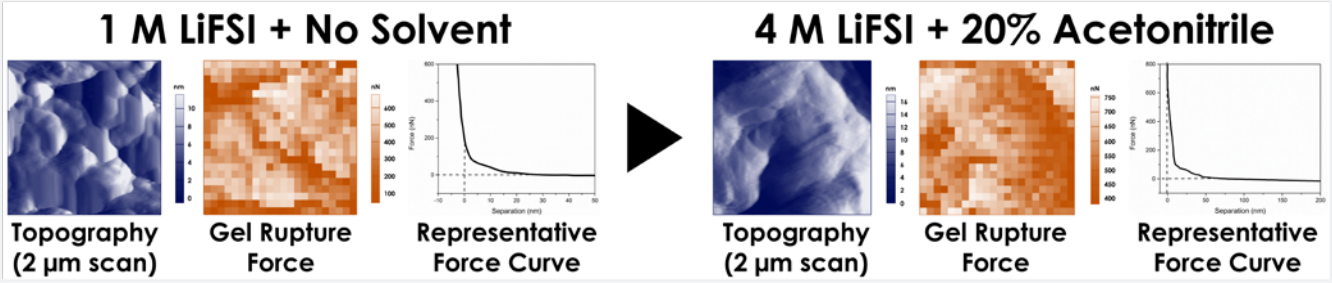

Figure 5. Polymer gel electrolyte morphology and mechanical properties as a function of Li salt concentration (1 M or 4 M) and acetonitrile (present or absent). *(adapted from reference 2)*

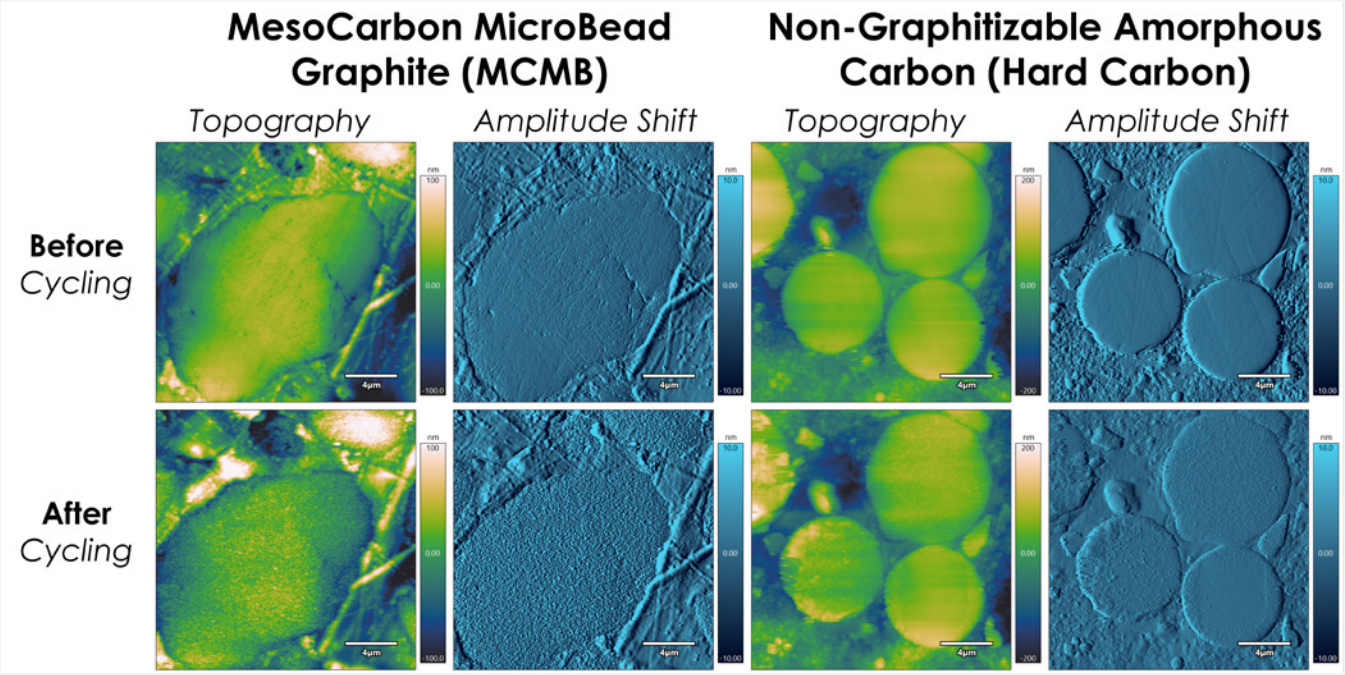

Figure 6. SEI formation on MCMB and Hard Carbon electrodes during in-situ voltage cycling. *(adapted from reference 3)*

The HOPG electrode also exhibited blistering, a common effect seen in ethylene carbonate (EC) electrolytes with trace H_2O molecules that are co-intercalated and subsequently electrolyzed to gas between the graphitic layers. As can be seen in **Figure 7**, showing 20 µm scans at the start and end and 5 µm scans during a full cyclic voltammogram under these conditions, the SEI first forms during the sweep to lower voltages (**Figure 7A-E**), followed by blistering as the voltage is swept back to higher potentials where the intercalated water molecules are split (**Figure 7F-I**).

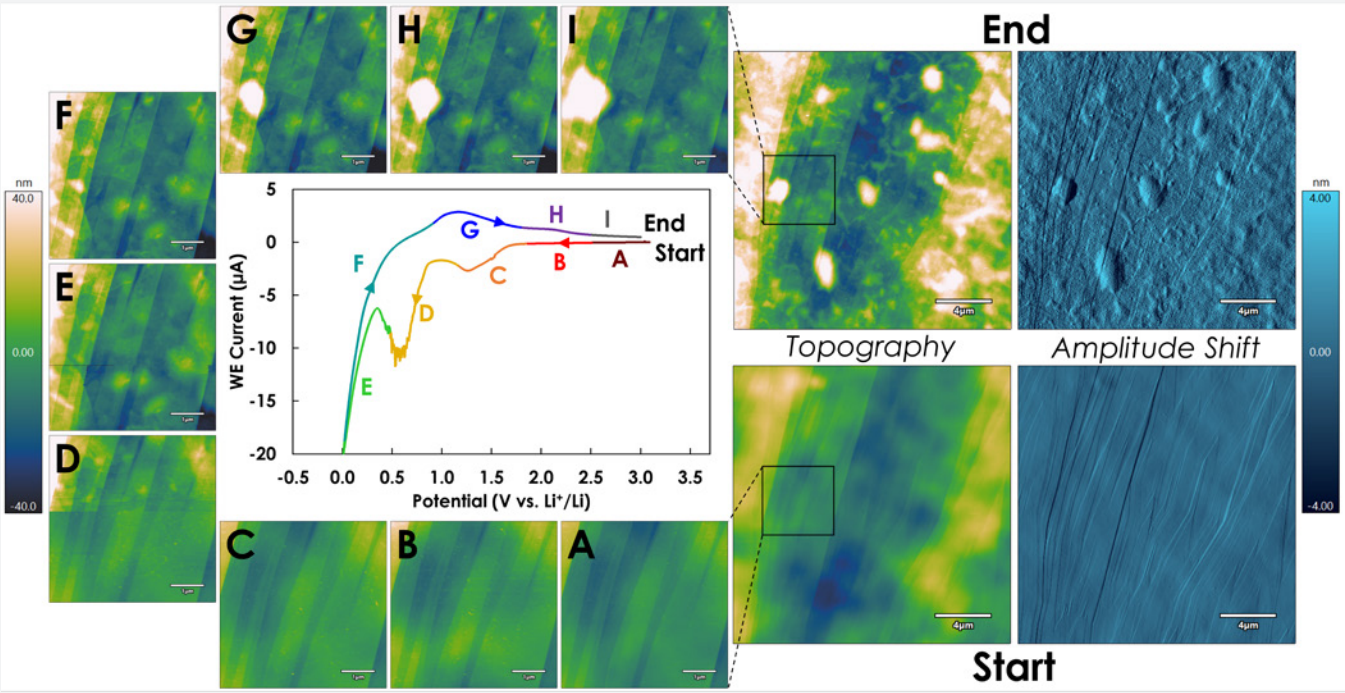

Figure 7. SEI formation during voltage cycling on a HOPG electrode. Colored segments labelled A through I in the central Cyclic Voltammogram correspond to the voltage ranges during which the corresponding images labelled A through I were acquired. *(adapted from reference 3)*

It is noteworthy that in the AFM image in **Figure 7D**, the SEI suddenly comes into view while scanning up the image, corresponding to the steep faradaic current spike during segment D (yellow) in the cyclic voltammogram. For the start/end 20 µm scans, amplitude shift data is also included to showcase the dramatic change in roughness from the SEI formation during the cycle.

Example: Zinc as an electrode material

Another in-situ measurement example considers zinc as the negative electrode material in rechargeable batteries. Zinc may be familiar as the coating on galvanized nails, wherein it acts as a sacrificial anode to prevent corrosion of the underlying steel. It is also currently used in single-use zinc-air hearing aid batteries due to its excellent shelf life, low cost, and high energy density. For those reasons, it is an attractive negative electrode material in rechargeable batteries, but making the zinc functionally rechargeable requires optimization because it is prone to dendrite or filament formation that can result in catastrophic short circuiting.

discharging. Repeated cycling would correspond to repeated cycles of the growth and dissolution of these crystal structures. In the series of images in **Figure 8**, Zinc film growth was monitored in situ using voltage control in an electrochemical cell inside the AFM, while dry Argon gas was flowed through the cell to remove moisture. These images reveal that film topography (roughness) generally increases as a function of film thickness (charging time). Following this, by varying the applied overpotential between three different voltages (225, 325, or 425 mV), it is observed that the film roughness changes differently as a function of charging time: at 325 mV overpotential (blue data points), roughness levels off to a constant value, indicating that the film is being uniformly deposited and dendrite formation is therefore being mitigated. These are the ideal nanoscale conditions that can now be translated to rechargeable Zn battery operation.

A recent subsequent study helped confirm the formation of hexagonal Zn platelets and their growth and coalescence over time.[5] These data,

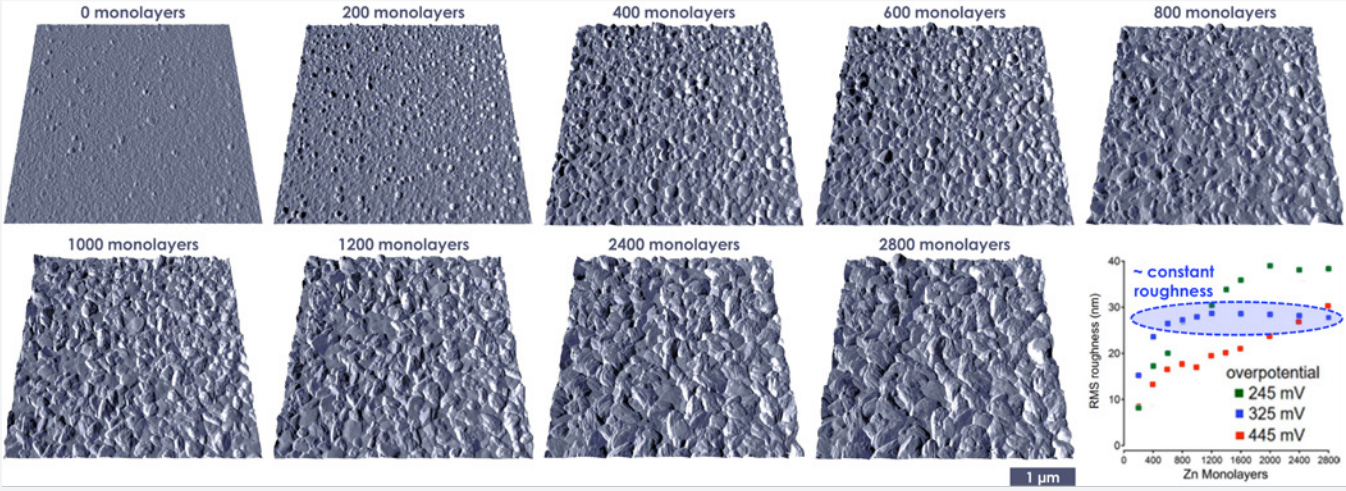

Figure 8. Electrodeposition of polycrystalline zinc from ionic liquid electrolytes onto the negative electrode. *(adapted from reference 4)*

Researchers from Lawrence Livermore National Lab have therefore been characterizing the electrodeposition (plating) of polycrystalline zinc from ionic liquid (IL) electrolytes in hopes of improving rechargeability, as ILs have been shown to reduce Zn dendrite formation.[4] Electrodeposition specifically represents the growth of Zn crystals during the charging process for the negative terminal of the battery, and the crystals would correspondingly dissolve if the battery was

not shown here, helped interpret in-situ ultra-small-angle X-ray scattering (USAXS) data and was further corroborated with ex-situ Scanning Electron Microscopy. These results showcase the utility of AFM for correlating nanoscale measurements even across measurement platforms, and they provide a more complete picture of Zn electrodeposition that improves cyclability of Zn-electrode batteries and therefore makes them more commercially practical.

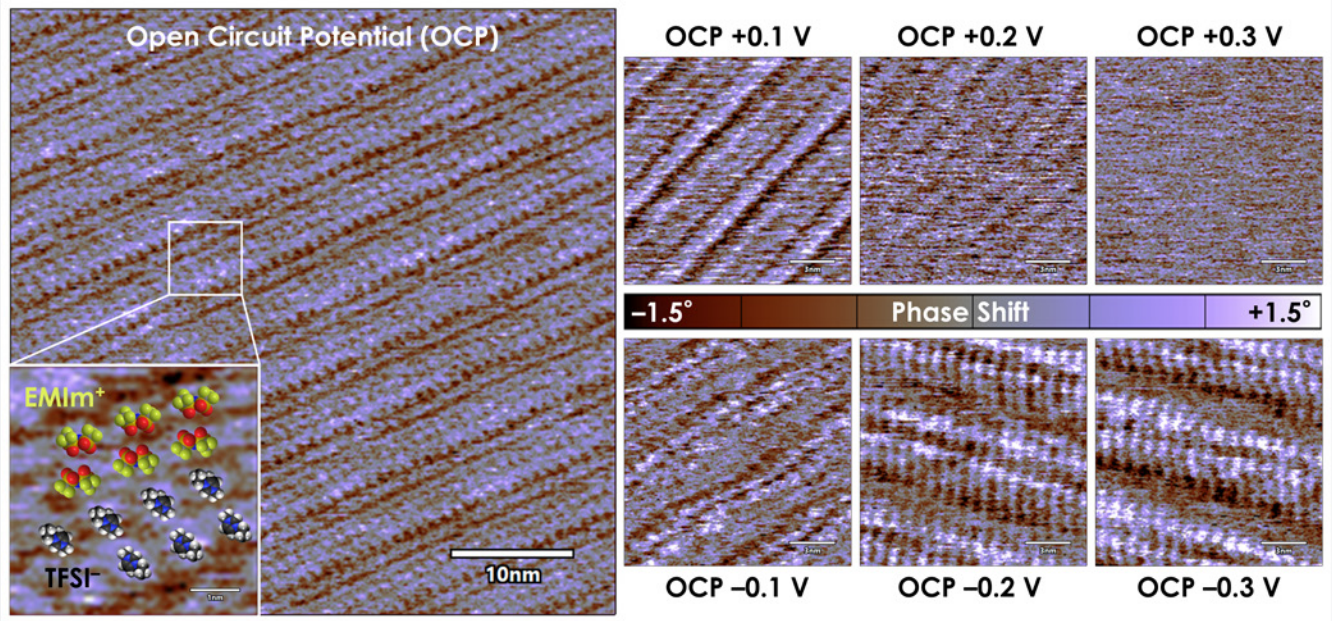

Figure 9. As seen with tapping mode phase mapping, applying a potential to the graphite electrode surface significantly alters the EMIm+ / TFSI– ionic liquid Stern layer nanostructure. *(adapted from reference 6)*

Example: Ionic liquid conformation changes at a biased electrode

Phase mapping is one of the most sensitive outputs of tapping mode imaging, as changes in phase are related to changes in the energy dissipated into the sample due to stiffness variations. If we zoom into the sub-micron imaging scale, phase mapping amounts to being able to distinguish chemical moieties in surface-assembled 2D van der Waals adlayers and molecular crystals.

Ionic liquids (ILs) have attracted attention for use in battery electrolytes because of their large electrochemical stability windows, low volatility, high thermal stability, and high conductivity. They are relatively large, polar, organic molecules (and in this case, "large" means about 1 nm in size), but they do not behave like typical salt solutions—especially at the electrode interface—and this can affect device performance. Ionic liquids are thought to be molecularly "templated" at surfaces, meaning they form well-ordered Stern layers.

In one study researchers employed the extreme sensitivity of phase mapping to evaluate the molecular ordering properties of the IL known as 1-ethyl-3-methylimidazolium bis(trifluoromethylsulfonyl)imide ($EMIm^+$ / $TFSI^-$) at a biased graphite electrode.[6] Measurements at this scale provide a view into phenomena that might transpire at the first few atomic or molecular layers adjacent to the cathode or anode surface inside of a battery while it is charging or discharging.

The resulting data allow direct visualization of the molecular ordering on a graphite surface by taking advantage of Cypher's ultra-high resolution capabilities (**Figure 9**, noting the scale bars). Using a potentiostat and electrochemical cell, the potential at the graphite electrode surface can be varied and the Stern layer significantly altered its structure as it compensated for interfacial charge. That is, the surface is enriched with anions at positive potentials, and enriched with cations at negative potentials, and the ionic liquid molecules rearrange to make space for these ions as they migrate to the surface. In the image at far left in **Figure 9**, the molecular ordering with no applied bias (open circuit potential) is apparent, showing the regular patterning of $EMIm^+$ and $TFSI^-$. In the images at right in **Figure 9**, structural rearrangements and even loss of order are apparent as the magnitude of applied voltage increases: In the top row, as the applied voltage increases to +300 mV above open circuit, the structural order completely disappears, while a -300 mV bias changes the periodicity of the Stern layer.

In addition to solvent behavior, these molecular scale phenomena likely also occur at electrodes in newer battery technologies such as Redox Flow Batteries where outer-sphere electron transfer to metal ions and soluble redox-active organic molecules in solution allows energy to be stored in tanks of liquid rather than through plating, stripping, or ion intercalation into solid materials. These Stern-layer data no doubt have implications for interfacial charge transfer that ultimately affects battery operation.

Example: Separator Correlative Mapping

Most batteries require a separator, or ion-conducting membrane, between the materials on the positive and negative terminals. These separators prevent chemical crossover between terminals, but add cost and increase internal resistances in practical devices. The internal resistance is often related to the chemical moieties of the material as well as its molecular structure and resulting ionic conductivity.

AFM phase mapping is again a very sensitive imaging technique for analyzing the separator microstructure because hydrophobic and hydrophilic domains have different energy dissipation and therefore phase response. In one study, researchers used phase mapping and electrostatic force microscopy (EFM) to determine that separators with fibers parallel to the plane of the separator have a higher EFM response and lower ionic conductivity and connectivity, while separators with perpendicular fibers resulted in lower EFM response and higher ionic conductivity and connectivity (data not shown here).[7]

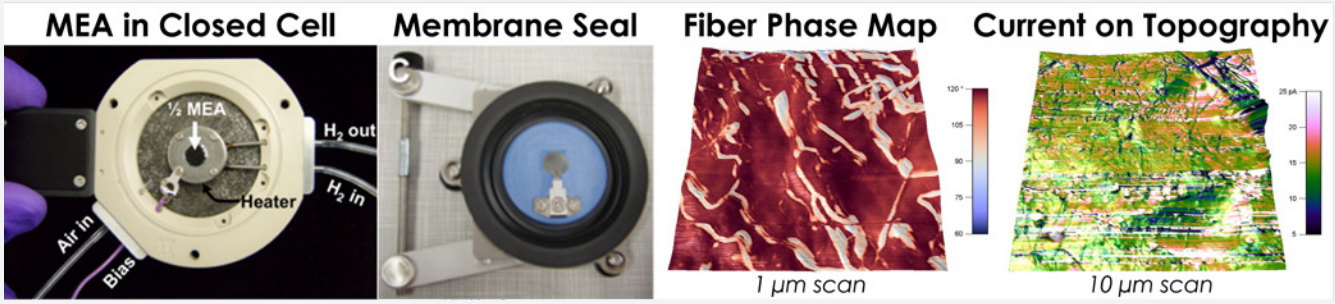

Figure 10. Phase and Conductive AFM mapping on a wetted anionic exchange membrane separator. *(adapted from reference 8)*

In a second study the same group used a similar, commercially available ion exchange membrane and this time correlated its topography in hydrated and dehydrated states to electrical conductivity that corresponds to the transference of hydroxide ions through ion channels.[8] For these measurements, a membrane electrode assembly (MEA) was mounted inside the MFP-3D AFM closed cell that allows for air and hydrogen gas flow, bias, and temperature control all inside the cell for in-situ testing, and this seals with a membrane around the cantilever holder (**Figure 10**). The AFM tip detects nA-scale currents from ionic flows through conducting channels in the separator. At dehydrated conditions, AFM phase images indicated that relatively few hydrophilic domains existed, owing to a lack of water retention from the hydrophobicity of the polymer, meaning that the separator would be poorly conductive. As the hydration increased, phase maps showed a surface structure change where randomly dispersed and isolated fibrillar hydrophilic domains were present, an encouraging finding. However, following this with conductive AFM measurements revealed that the increase in hydrophilic domains did not result in an increase in conductivity: these elongated structures were insulating (**Figure 10, Current**), suggesting that the high water content of the membrane induces surface rearrangement and excessive swelling, but not ion conductance. These results have bearing on the choice of separator one might choose to use inside a battery.

Operando AFM measurements

Example: Operando imaging of the positive terminal of a Li-oxygen battery

Increasing the complexity and difficulty of the measurement to its maximum, consider an operating battery with an extremely sensitive chemistry: lithium-oxygen. If this type of battery becomes optimized, it will likely be implemented in fast-charging and long-range cars and other high-performance devices. For this study, the Li-O_2 battery was assembled inside the AFM so that the positive electrode surface (glassy carbon) was accessible by the AFM probe in a 1 M $LiNO_3$ tetraglyme electrolyte, while the sealed sample chamber of the Cypher ES AFM was purged with pure oxygen gas.[9] The oxygen gas flow was remarkable because the AFM was operating inside an argon-filled glovebox and the oxygen critically did not escape into the glovebox atmosphere due to the hermetic seal of the Cypher ES sample cell.

As can be seen in **Figure 11**, tapping mode topography data corresponding to a full discharge-charge cycle of this lithium-oxygen battery was obtained. The negative electrode is solid lithium metal, and the positive electrode is polished glassy carbon where oxygen reacts during discharge and where the AFM probe is scanning to acquire images of the Li-oxygen reaction products. Current was

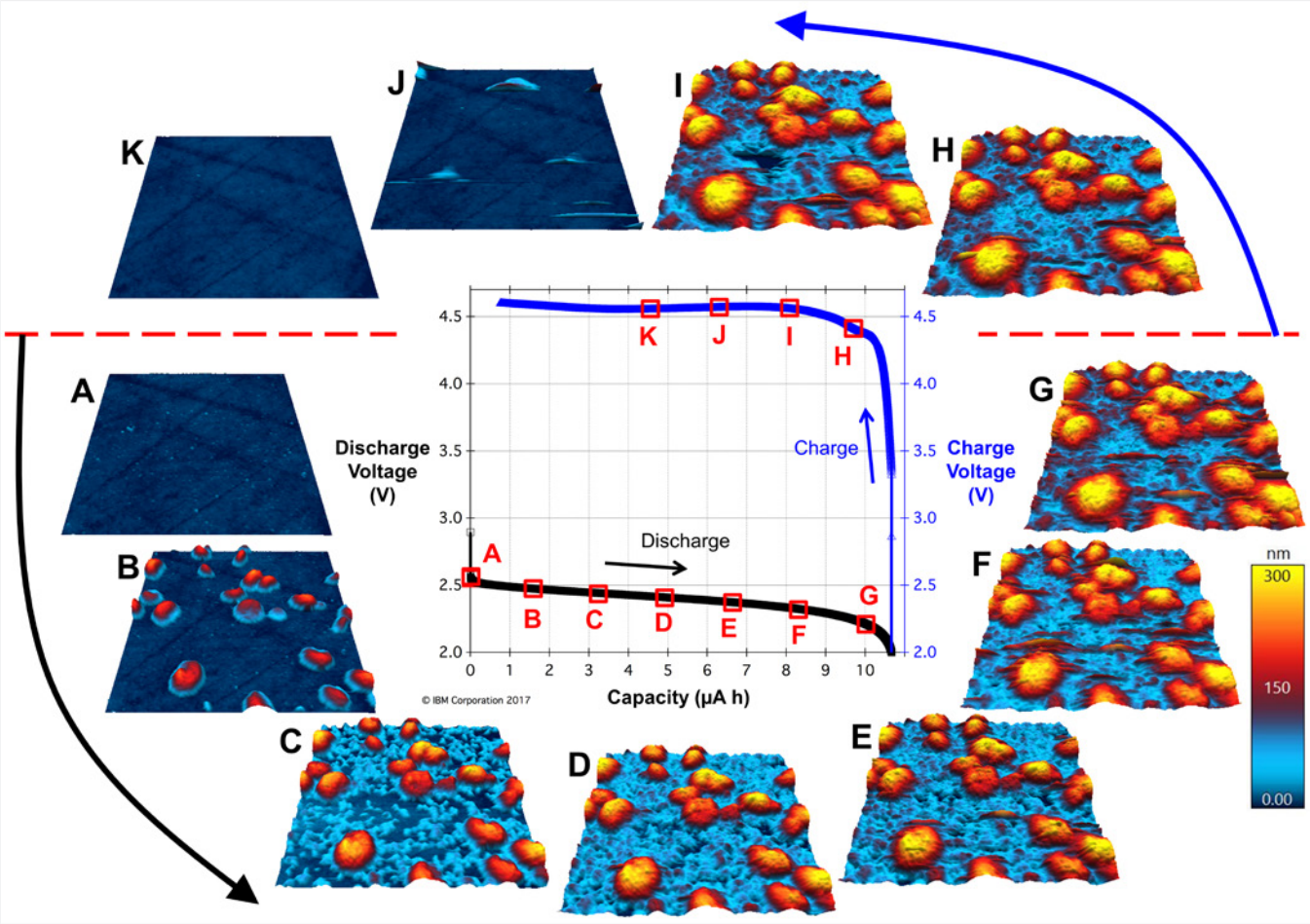

Figure 11. Operando imaging of mixed-valence LiOx deposits on the glassy carbon positive electrode during a full charge/discharge cycle of a Li-O_2 battery *(adapted from reference 9)*

controlled to 2 μA during both the charging and discharging portions of the cycle, corresponding to a full cycle time of just over 10 h, and the AFM imaging was stable the whole time. In the center is a plot of the battery's capacity vs. output voltage during the cycle, and around the outside are 3-micron AFM topography images obtained during the cycle—that is, operando imaging. As the battery discharges (**Figure 11A-G**), lithium atoms oxidize and become mobile in the solvent. A mixed-valence lithium-oxygen (LiO_x)solid-electrolyte interphase material then nucleates, grows, and coalesces into a conformal coating on the glassy carbon, visualized here as the red-yellow structures in the AFM images. Upon charging (**Figure 11H-K**), the structures initially persist, then begin to dissolve, and finally disappear by the time 50% state of charge is reached at point K. One key conclusion here is that the coalesced LiO_x discharge layer is structurally stable during discharge and completely dissolves during subsequent charging, and this indicates that this battery should be highly cyclable. AFM was the only way to observe the structural evolution and persistence of this layer during battery operation.

Example: CO_2 Catalysis at a Copper Electrode

This final example is technically a divergence from batteries but remains relevant because a driven electrochemical process is being monitored in an operating catalytic cell inside the AFM. While not an energy storage device, this still represents energy storage because electrons are being used for reductive chemical bond formation that is naturally extensible to the charge/discharge energy conversion phenomena at battery electrodes.

The first observation in this study, is that after the surface is wetted with electrolyte, it rapidly forms epitaxial copper-oxide platelet structures with hexagonal symmetry.[10] Even in this advanced experimental setup, the Cypher ES AFM maintains its ultra-high resolution, mapping the atomic lattice of the Cu-oxide platelets and revealing their hexagonal periodicity and rhomboidal unit cell (**Figure 12A**).

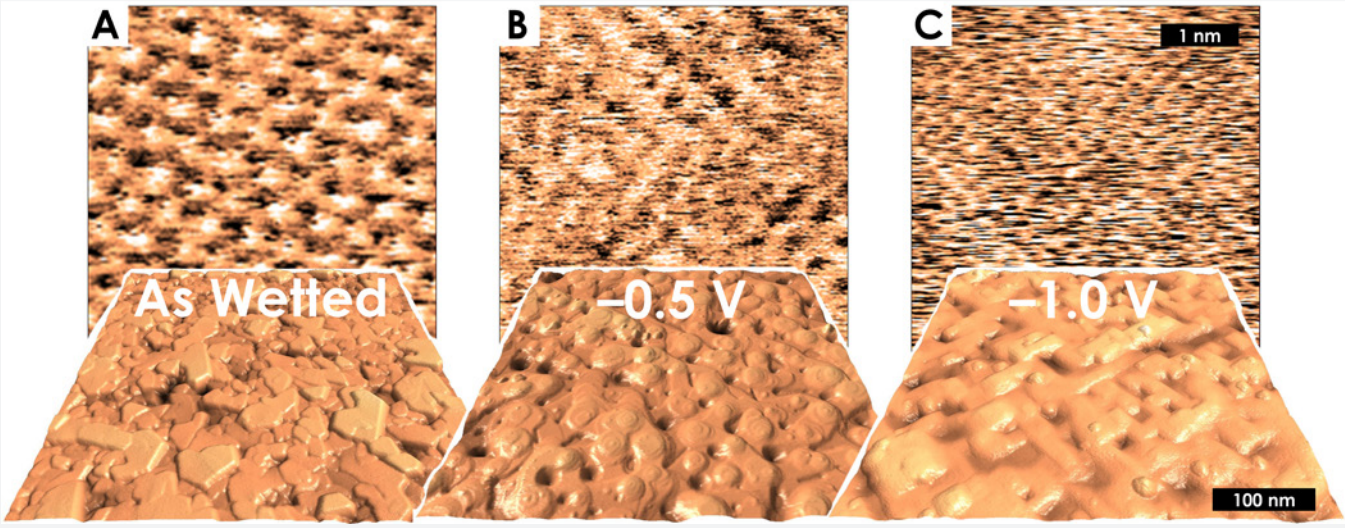

Figure 12. In-situ voltage-dependent atomic and sub-micron morphology of crystalline Copper during catalytic CO_2 electroreduction. (A) $Cu_2O(111)$ platelets and atomic resolution in the as-wetted state at open circuit potential. (B) "Mound-pit" topography and 2x2 lattice structure at –0.5 V. (C) "Straight terrace" topography and 1x1 lattice structure at –1.0 V. *(adapted from reference 10)*

Next, a potentiostat was used to modulate the applied voltage and drive CO_2 reduction. As the voltage became more negative, the surface topography of the copper transitioned from the as-wetted platelet structures to a mound-pit structure with round edges at -0.5 V and then a straight terrace structure with 90 degree angles as the voltage was brought even lower to -1.0 V (**Figure 12B,C**). Zooming in on the resulting crystalline facets, a remarkable atomic structure transition also emerges where there appears to be a molecular carbon-monoxide adlayer making a 2x2 structure at -0.5 V, while the atomic structure returns to 1x1 at -1.0 V (**Figure 12B,C**). Amazingly, these experimental conditions also evolve gas due to water hydrolysis, but despite the formation of gas bubbles, the AFM was still able to acquire these ultra-high resolution images.

These results directly reveal the intricate interplay between catalyst preparation and handling, morphology and structure, defect nature and density, applied potential, and electrolyte. It is often assumed that the surface is metallic copper under CO_2-reducing conditions, but this work shows that surface reconstructions, oxides, and even molecular adlayers at relevant applied potentials must be considered to establish catalyst structure-property relationships. Here, the voltammetric behavior of the copper surface is also nano-structure sensitive, and these operando results were the only way to confirm these phenomena. It is expected that these data and nanoscale transformations will have analogs in other electrochemical and catalytic systems.

Conclusion

In this whitepaper, we have shown only a select few examples of how to characterize batteries and electrochemical interfaces with ex-situ, in-situ, and operando measurements with AFM. Key aspects to take away from this are that Asylum Research AFMs are both a unique and versatile tools for characterizing the individual components and reactive interfaces inside batteries. Experiments can be performed with voltage control, inside an electrochemical cell, inside the AFM, and further environmentally controlled by using a glovebox owing to the exceptional stability and low noise of the Cypher ES AFM. AFM provides insight into roughness, morphology, mechanical criteria, molecular ordering, and much more that can be critical for monitoring reaction progress, optimizing reaction conditions and interfacial charge transfer, or simply qualifying battery components before assembly.

References

1) https://www.statista.com/statistics/1103218/global-battery-demand-forecast/

2) Lahiri, A., Pulletikurthi, G., Shapouri Ghazvini, M., Höfft, O., Li, G., & Endres, F. (2018). Ionic Liquid–Organic Solvent Mixture-Based Polymer Gel Electrolyte with High Lithium Concentration for Li-Ion Batteries. The Journal of Physical Chemistry C, 122(43), 24788-24800.

3) Luchkin, S. Y., Lipovskikh, S. A., Katorova, N. S., Savina, A. A., Abakumov, A. M., & Stevenson, K. J. (2020). Solid-electrolyte interphase nucleation and growth on carbonaceous negative electrodes for Li-ion batteries visualized with in situ atomic force microscopy. Scientific reports, 10(1), 1-10.

4) Keist, J. S., Orme, C. A., Wright, P. K., & Evans, J. W. (2015). An in situ AFM study of the evolution of surface roughness for zinc electrodeposition within an imidazolium based ionic liquid electrolyte. Electrochimica Acta, 152, 161-171.

5) Keist, J. S., Hammons, J. A., Wright, P. K., Evans, J. W., & Orme, C. A. (2020). Coupling in situ atomic force microscopy (AFM) and ultra-small-angle X-ray scattering (USAXS) to study the evolution of zinc morphology during electrodeposition within an imidazolium based ionic liquid electrolyte. Electrochimica Acta, 342, 136073.

6) Elbourne, A., McDonald, S., Voichovsky, K., Endres, F., Warr, G. G., & Atkin, R. (2015). Nanostructure of the ionic liquid–graphite stern layer. ACS nano, 9(7), 7608-7620.

7) Barnes, A. M., Du, Y., Liu, B., Zhang, W., Seifert, S., Coughlin, E. B., & Buratto, S. K. (2019). Effect of Surface Alignment on Connectivity in Phosphonium-Containing Diblock Copolymer Anion-Exchange Membranes. The Journal of Physical Chemistry C, 123(51), 30819-30826.

8) Barnes, A. M., Liu, B., & Buratto, S. K. (2019). Humidity-dependent surface structure and hydroxide conductance of a model quaternary ammonium anion exchange membrane. Langmuir, 35(44), 14188-14193.

9) Virwani, K., Ansari, Y., Nguyen, K., Moreno-Ortiz, F. J. A., Kim, J., Giammona, M. J., ... & La, Y. H. (2019). In situ AFM visualization of Li–O_2 battery discharge products during redox cycling in an atmospherically controlled sample cell. Beilstein journal of nanotechnology, 10(1), 930-940.

10) Simon, G. H., Kley, C. S., & Roldan Cuenya, B. (2021). PotentialDependent Morphology of Copper Catalysts During CO_2 Electroreduction Revealed by In Situ Atomic Force Microscopy. Angewandte Chemie International Edition, 60(5), 2561-2568.